A chaotic model for the epidemic of Ebola virus disease in West Africa (2013–2016)

Sylvain Mangiarotti, Marisa Peyre, and Mireille Huc

Citation: Chaos **26**, 113112 (2016); doi: 10.1063/1.4967730
View online: http://dx.doi.org/10.1063/1.4967730
View Table of Contents: http://scitation.aip.org/content/aip/journal/chaos/26/11?ver=pdfcov
Published by the AIP Publishing

Articles you may be interested in

Computational model of a vector-mediated epidemic
Am. J. Phys. **83**, 468 (2015); 10.1119/1.4917164

Epidemic spreading in time-varying community networks
Chaos **24**, 023116 (2014); 10.1063/1.4876436

Evolution of N-species Kimura/voter models towards criticality, a surrogate for general models of accidental pathogens
AIP Conf. Proc. **1479**, 1331 (2012); 10.1063/1.4756401

The impact of awareness on epidemic spreading in networks
Chaos **22**, 013101 (2012); 10.1063/1.3673573

Generalized entropies of chaotic maps and flows: A unified approach
Chaos **7**, 694 (1997); 10.1063/1.166267

Reuse of AIP Publishing content is subject to the terms at: https://publishing.aip.org/authors/rights-and-permissions. Downloaded to IP: 193.51.119.103 On: Thu, 08 Dec 2016 14:23:21

A chaotic model for the epidemic of Ebola virus disease in West Africa (2013–2016)

Sylvain Mangiarotti,[1] Marisa Peyre,[2] and Mireille Huc[1]
[1]*Centre d'Études Spatiales de la Biosphère, CNRS-UPS-CNES-IRD, Observatoire Midi-Pyrénées, 18 Avenue Édouard Belin, 31401 Toulouse, France*
[2]*UPR AGIRs, Bureau 208, Bâtiment E TA C22/E, Centre de Coopération Internationale en Recherche Agronomique pour le Développement (CIRAD), Campus International de Baillarguet, Montpellier Cedex 5 34398, France*

(Received 9 August 2016; accepted 28 October 2016; published online 16 November 2016)

An epidemic of Ebola Virus Disease (EVD) broke out in Guinea in December 2013. It was only identified in March 2014 while it had already spread out in Liberia and Sierra Leone. The spill over of the disease became uncontrollable and the epidemic could not be stopped before 2016. The time evolution of this epidemic is revisited here with the global modeling technique which was designed to obtain the deterministic models from single time series. A generalized formulation of this technique for multivariate time series is introduced. It is applied to the epidemic of EVD in West Africa focusing on the period between March 2014 and January 2015, that is, before any detected signs of weakening. Data gathered by the World Health Organization, based on the official publications of the Ministries of Health of the three main countries involved in this epidemic, are considered in our analysis. Two observed time series are used: the daily numbers of infections and deaths. A four-dimensional model producing a very complex dynamical behavior is obtained. The model is tested in order to investigate its skills and drawbacks. Our global analysis clearly helps to distinguish three main stages during the epidemic. A characterization of the obtained attractor is also performed. In particular, the topology of the chaotic attractor is analyzed and a skeleton is obtained for its structure. *Published by AIP Publishing.* [http://dx.doi.org/10.1063/1.4967730]

Mathematical models can offer useful insight to analyze and forecast the evolution of epidemics in expansion. A generalized version of the global modeling technique is introduced here and applied to the epidemic of Ebola Virus Disease (EVD) that broke out in West Africa in December 2013. The analysis clearly permits to distinguish three main stages during the outbreak: (i) the earlier development of the epidemic in remote regions, (ii) the uncontrolled period of rapid propagation of the disease in urban regions, and (iii) its long slowdown until it could end. The obtained model shows that the epidemic is governed by a low-dimensional chaotic dynamics. The resulting four-dimensional chaotic attractor is analyzed in terms of the dynamical, geometrical, and structural properties. To characterize the topology of this attractor, a skeleton is proposed for its four-dimensional chaos.

I. INTRODUCTION

When an epidemic is in expansion, it is important to have approaches that can be applied to scarce data sets. This is especially true for emerging and reemerging diseases, for which causes and transfer processes are often poorly known and understood. It is also the case for epidemics of well understood diseases for which dynamics may vary from one focus to another, and more especially when the disease is characterized by high levels of lethality. Ebola virus and Marburg diseases are among these.

Most of the models developed to simulate infectious diseases are issued from the pioneering work of Kermack and McKendrick[1] initially designed to model plague epidemics. These models divide the population in compartments that generally distinguish Susceptible, Infected, Recovered and possibly also Exposed and other classes of a given population. Compartment models can be applied to one or several species and thus to epidemics, epizootics, and coupled epidemics and epizootics. Such models have proven to be useful to better understand the epidemics, and can be used today to model the Ebola virus epidemic.[2–5] Nevertheless, modeling epidemics in general, and Ebola epidemics in particular, remains a quite difficult problem, in particular, because of the large variability of dynamics that can be observed from one outbreak to another. Such diversity appears flagrant for Ebola virus epidemics when comparing the West Africa Ebola outbreak of 2014[6] (for which total number of reported cases and deaths are extremely high, 28 652 and 11 325, respectively) to any of the outbreaks that occurred previously or concurrently in central Africa[7] ($\leq$425 infections and $\leq$280 deaths, laboratory confirmed cases only).

Such monitoring is especially difficult for emerging diseases for which it is sometimes required to consider simultaneously unprecedented humanitarian crisis together with the fundamental and applied scientific challenges in order to identify the various reservoirs contributing to the propagation of the disease and to understand the processes at work, with the aim to slow down and if possible to stop the epidemic. The large number of factors involved in a disease

Reuse of AIP Publishing content is subject to the terms at: https://publishing.aip.org/authors/rights-and-permissions. Downloaded to IP: 193.51.119.103 On: Thu, 08 Dec 2016 14:23:21

generally make the task particularly complex, since it includes a wide diversity of intertwined problems of diagnostics, management, biology, ecology, society, economic, environment, etc. Such problems are all present in an epidemic such as Ebola[6,8] and especially difficult to take into account in a modeling approach.

Since often facing a strong non-stationarity of the dynamical behavior—in space and in time—it would be useful to develop pragmatic approaches for such contexts. Indeed, it is necessary to explore the alternative methods to forecast the time evolution of the disease that, for instance, would help for the estimation of the urgent needs in a more pragmatic way.

This may be done by directly fitting compartment models to the data in order to adapt the models to the current context. Indeed, processes modeling can be very useful to better understand the dynamics of a disease. An *ad hoc* calibration of such models may provide useful simulations but it requires its algebraic formulation to be well adapted to the dynamical context. Unfortunately, a proper calibration may require a complete set of local information to parameterize the model appropriately. In many cases, local information is missing, and it is necessary to reuse information from other sites of study and/or previous outbreaks, assuming stationary conditions in space and time. Such assumption can be hazardous since a information can exhibit an important variability in space and time.[9] Note that model parameters can also depend on the aggregation scale[10] and thus on the model spatial representativity. This problem can be met when transporting the model from one outbreak to another.

Moreover, the variations of the algebraic structure required to model the epidemics can be very different, not only from one type of disease to another, but also between several focuses of the same disease. This hypothesis of ergodicity is often very partially satisfied only, and thus hard to justify. It is especially the case when considering emergent diseases such as Ebola for which important factors remain poorly known. In the case of the West Africa Ebola epidemic, heterogeneous behaviors could be observed both in space and time.[11] It is quite important to take this difficulty into account when attempting to model an epidemic in expansion, especially in a context of scarce data.

The global modeling technique may be a useful and complementary technique to explore epidemics in such conditions. This technique is based on the theory of nonlinear dynamical systems that allows a deterministic and strongly nonlinear point of view fully adapted to analyze the dynamics presenting limited horizons of predictability.

Several models were already obtained from the environmental data based on this technique.[12,13] Note that a model of difference equations could also be obtained for the whooping cough in London for the period from 1967 to 1990.[14] Recently, the approach was applied to a multivariate set of variables to model the epidemic of plague that occurred in Bombay at the end of the 19th century.[15] In this latter work, it was shown that it was possible to identify the couplings of the epidemic of plague with the epizootics of the two main species of rats.

The objective of the present work is to investigate the capacity of the global modeling technique to model an epidemic of EVD based on a restrictive number of observables, during the very strong propagation of the disease. The West Africa epidemic (2013–2016) is considered in this study. Although the whole period for which data are available is considered in the analysis, the modeling part is focused on the period between March 2014 and January 2015, that is, before any clear breakdown of the epidemic.

Data used in the study and their epidemiological context are presented in Section II. The global modeling technique is introduced in Section III. To make it applicable to a couple of observables, a generalized formulation of the approach is introduced. Results are presented in Section IV. Discussions and conclusions are given in Section V.

II. DATA AND CONTEXT

A. General background

EVD is due to an etiological agent of the family of *Filoviridae*. It is one of the most serious viral disease currently known, for which no prophylactic or therapeutic strategies were found. Five species of the Ebola virus are identified among which Ebola-Zaire strain has the highest level of lethality, with a rate close to 70%.[9]

Fruit bats are considered to be the most likely carriers of the Ebola virus in the wild.[16] Three main species of fruit bats (*Hypsignathus monstrosus*, *Epomops franqueti*, and *Myonycteris torquata*) have been identified as potential carriers, their geographic distribution covers a large area from Central to West Africa.[16] Interestingly, the potential spread of the EVD had already been estimated based on the ecological niche modeling in earlier works.[17] Although outbreaks remain quite rare, it is estimated that 22×10^6 of people live in areas at risk,[18] that makes the transmission of Ebola virus from animal to man possible. Alteration of the biosystems by land-use change and deforestation has been intensive in this region, where mosaics of forest and agriculture are now dominating the countryside.[19] This evolution may have increased the probability of contact between chiroptera and human.

Transfer of the Ebola virus from animals to humans and between humans can typically occur through contact with bodily fluids of infected animals and humans. This transfer may occur during the butchering of bats,[20] when consuming infected bushmeat, when caring for patients[21] or when preparing the deceased for burial.[5,21,22] The detection of the disease is made difficult by the fact that most of the symptoms of the disease are not specific, and thus difficult to distinguish from other diseases such as yellow fever and malaria, also endemic to the region.[8]

B. Comparative contexts

It was established that the epidemic of EVD that has swept West Africa from 2013 to 2016 had no link with the previous epidemics.[23] Since the strain of the virus was identified as *Zaire ebolavirus* (one of the strains responsible for several of the previous outbreaks in Central Africa), a similar behavior could have been expected. It was definitively not

Reuse of AIP Publishing content is subject to the terms at: https://publishing.aip.org/authors/rights-and-permissions. Downloaded to IP: 193.51.119.103 On: Thu, 08 Dec 2016 14:23:21

the case and several important elements were evoked to explain such a strong differentiation. One important reason may probably be that most of the previous outbreaks occurred in remote forested areas that are places of low population density with slow connections by road, river, and air, thus limiting human contacts. Another quite probable reason may be that an important experience of EVD epidemics has been acquired in Central Africa.[23] This was clearly not the case in West Africa where health services were found sharply unprepared,[11] due to both the devastating effect of civil wars in Liberia and Sierra Leone and the very difficult economic situation in the three involved countries which are among the poorest countries in the world.[24] These elements have probably played an important role in the present context, although other factors can also have contributed to this differentiation.

C. Data source and preprocessing

One important objective of the present work is to test the efficiency of the global modeling technique to obtain a model based on scarce information (two observables only). Two time series are used: the number of people infected by the Ebola virus and the number of resulting deaths. Data are from the World Health Organization and were downloaded from the Centers for Disease Control and Prevention.[25] These data are reported as cumulative numbers starting from the beginning of the epidemic and have an irregular sampling time (Fig. 1(a), dotted values). Since, almost all (>99.7 %) Ebola cases of infections and deaths belong to the same geographical region (a large scale area including Guinea, Liberia, and Sierra Leone), values basically resulting from the addition of these three countries are used to perform the analysis. The time window used for the modeling focuses on year 2014, from the 23rd of March 2014 to the 21st of January 2015 (from day 107 to day 411 after the index case that was identified to take place on the 6th of December 2013;[26] this date is the time reference of the epidemic used in the manuscript).

This time window thus includes the mostly active period of the epidemic, before any clear breakdown of the propagation could be detected. The evolution of the epidemics after January 2015 and until January 20th 2016 (day 775) will not be used for modeling but will be considered in the analysis for discussion.

These data[25] result from a real time data gathering process and may thus include modifications induced by reclassifications, new retrospective investigations, as well as time delay that will depend on laboratories availability.[27] For these reasons, data may exhibit inconsistencies. In the present case, some obvious contradictions were found quite located in time and/or relatively moderated in magnitude. Incoherences were fixed numerically by eliminating inconsistent values (corresponding to temporary decreases of cumulative number of infections or deaths): values corresponding to days 276, 320, 327, 329, 357, and 565 were thus removed. A preprocessing was then applied as follows: the two time series were re-sampled at a 1-day sampling using cubic splines. A damping function was applied to bound the

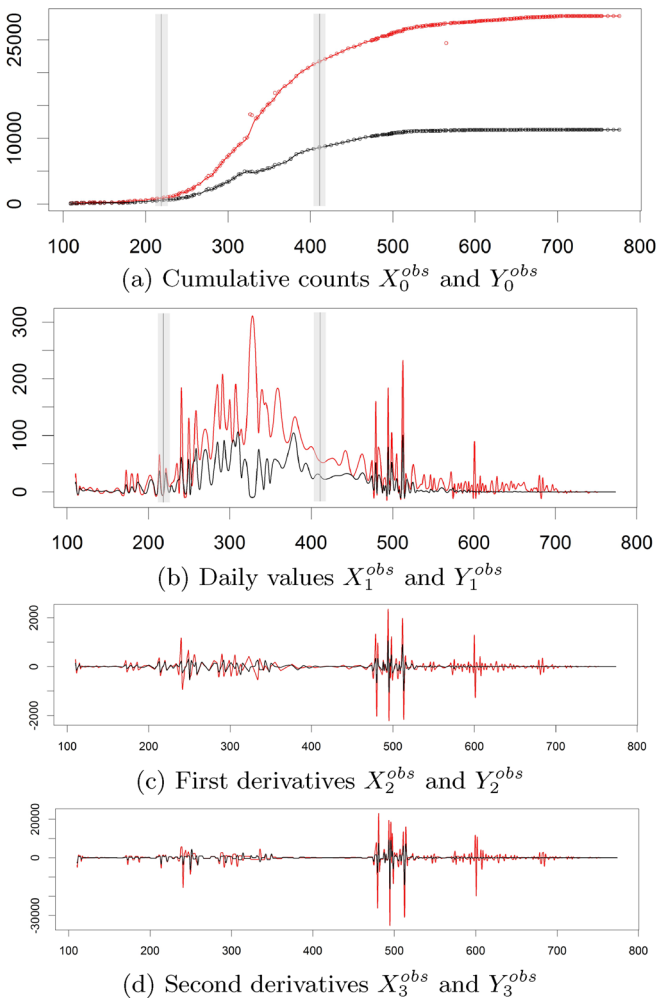

FIG. 1. Cumulative counts X_0^{obs} and Y_0^{obs} (a), daily numbers X_1^{obs} and Y_1^{obs} (b), and their first (c) and second (d) derivatives, of infections (in red) and deaths (in black) due to EVD for the West Africa epidemic for the region including Guinea, Liberia, and Sierra Leone. Date are given in day after the index case corresponding to December, the 6th of 2013.[26] Transitions between the three stages are reported as vertical bands. (For more convenience, note that January 1st corresponds to days 26 for 2014; 391 for 2015; 756 for 2016).

negative values closer to zero. The curves obtained for X_0 and Y_0 are presented in Figure 1(a) (plain line).

Daily numbers of infected cases and deaths were deduced from the previously preprocessed time series of cumulative number by computing the derivatives. The Savitzky-Golay filter[28] was used for this purpose and derivatives of higher degree, later required for applying the global modeling technique, were computed at the meantime (Figure 1). The time series of the daily numbers X_1^{obs} of infections and Y_1^{obs} of deaths present a high level of complexity with various time scales. The two variables X_1^{obs} and Y_1^{obs} have an overall coherent coevolution although not always correlated. Indeed, delayed oscillations and differentiated shapes and amplitudes can clearly be observed along the temporal signal. Their first and second derivatives are also reported (Figs. 1(c) and 1(d)). Despite the inherent limits previously evoked, the resulting time series appear coherent enough to apply our global modeling technique introduced in Section III.

Reuse of AIP Publishing content is subject to the terms at: https://publishing.aip.org/authors/rights-and-permissions. Downloaded to IP: 193.51.119.103 On: Thu, 08 Dec 2016 14:23:21

D. Stages of the West Africa epidemic

Three main stages during the propagation of this disease may be distinguished. The earlier stage (days ~ 0–220) corresponds to a period of moderate but complex expansion of the EVD in areas of low population density. Epidemiological look-back investigations allowed the identification of an index case who died on December 6th, 2013 in Meliandou, a small village of Guéckédou (Guinea).[26] The retrospective analysis revealed four linked clusters of infection and showed that the disease may have been spread from Guéckédou to Macenta (103 km from it), Nzérékoré (237 km) and Kissidougou (91 km) by a healthcare worker in February 2014.[26] The vicinity and the high porosity of the frontiers in the region, typical of West Africa, permitted the transfer of the disease from Guinea to Liberia and then to Sierra Leone. The hospitals and public health services in Guéckédou and Macenta (Guinea) alerted the Ministry of Health of Guinea on March 10th, 2014 about an unidentified disease of apparent high fatality rate. Blood samples were collected from hospitalized patients from which Ebola virus was identified. Until July 2014, a complex evolution of the epidemic in space and time was observed. In particular, later starts of quicker increases of the number of infections and deaths were noted in Liberia and Sierra Leone.[11] At this time, it seemed that the West Africa epidemic was contained.

Several unexpected new foci were found during July 2014, the epidemic had been underestimated and had become out of control. The second stage (days ~ 220–418) of the West Africa epidemic of EVD had already started. The Ebola Outbreak in West Africa was declared a "Public Health Emergency of International Concern" by the Emergency Committee in the beginning of August 2014.[29] This emergency was confirmed during the following weeks by an exponential increase of infections and death counts at the end of August (day ~ 265).[30] The quick spill-over of the disease was very likely due to a combination of problems that authorities had to face during the spread of the disease:[11] healthcare professionals were not trained to manage suspected and confirmed cases; organization to trace contacts between possibly affected individuals was not effective; resources and organization to follow new outbreaks of infections were insufficient; local community often exhibited a strong distrust towards control and prevention teams, and sometimes skepticism or even hostility, denying the access to medical teams. Since the virus quickly spread out from one district to another, even reaching numerous large cities including Conakry (Guinea) in March 2014, Monrovia (Liberia) in April 2014, Freetown (Sierra Leone) in July 2014 and others, new cases arose in multiple locations. It became especially difficult for the response team to follow all signaled cases and to trace them back. After an exponential increase observed at the end of August, the propagation speed reached the highest averaged levels ($X_1^{obs} > 100$ infections per day) which maintained during several months. The propagation rate appeared roughly regular in average (considering the cumulative counts) reflecting the relatively stationary conditions for the epidemiological dynamics during this period. A slight slowdown of the epidemic was temporarily observed at day ~ 380 but this detection remained local and uncertain at this date. Indeed, although incidences were estimated to be stable or declining in Liberia at the beginning of December (day 363),[31] it remained increasing in Guinea and Sierra Leone.[32,33]

It is only at the end of January 2015 that the focus could be considered as shifting from "slowing the transmission to ending the epidemic,"[34] corresponding to the third stage of the epidemic (day ~ 418-end). In practice, the limits between the different stages are difficult to define precisely. A decrease of strength was progressively observed. After day-~ 500, the number of deaths stabilized whereas the cumulative number of cases continued to increase slowly. Both variables almost completely stabilized after day ~ 700. The end of the epidemic was declared on June 9th, 2016.

III. METHODOLOGY

A. The global modeling technique

The global modeling technique aims to obtain models that can reproduce the global solutions of the dynamics, directly from time series, that is, without any other *a priori* information.[35,36] It can be applied to retrieve the Ordinary Differential Equations (ODE),[37,38] discrete equations,[39,40] or delayed equations.[36,41] In the present paper, only the continuous case of ODE is considered. When a single observable is available, the canonical form

$$\begin{cases} \dot{X}_i = X_{i+1} & \text{for } i = 1 \ldots (n-1) \\ \dot{X}_n = F(X_1, X_2, \ldots, X_n), \end{cases} \tag{1}$$

can be used, where X_i represents the $(i-1)$ th derivative of the observed variable X_1 assumed to be linked to the original variable x of the studied system such as $X_1 = h(x)$, with h the measurement function assumed bijective and smooth. Such an approach was successfully applied to numerous theoretical systems[37,38,42] and to the experimental data as well.[38,43,44] A three-dimensional model was obtained for lynx population in Canada.[12] Two three-dimensional models were obtained to model the cycles of cereal crops in North Morocco.[13] Interestingly, these latter models are the first models to provide an example of weakly dissipative chaos in nature. Indeed, all previous cases of weakly dissipative chaos are theoretical models that had not been obtained from the data.[45–47] Other examples of weakly dissipative 3D chaos were obtained for crops cycles in other Moroccan provinces.[48] These results contribute to prove that global modeling technique can be applied to a large spectrum of dynamical behaviors and to very different types of problems.

When several observables are available, the coupling between the observed variables can directly be investigated. In this case, the following form

$$\dot{X}_i = F_i(X_1, X_2, \ldots, X_n) \quad \text{for } i = 1 \ldots n, \tag{2}$$

may be expected.[15,48] Such formulation was shown to be a powerful approach to identify the couplings of the epidemic of plague in Bombay with the two epizootics of brown and black rats[15] by the end of 19th century. Surprisingly, it was found even possible to give a full interpretation of the

Reuse of AIP Publishing content is subject to the terms at: https://publishing.aip.org/authors/rights-and-permissions. Downloaded to IP: 193.51.119.103 On: Thu, 08 Dec 2016 14:23:21

obtained model. However, since only two observables are available in the present work, this latter formulation could only provide trivial solutions as proven by the Poincaré-Bendixon theorem. An alternative formulation must thus be used to obtain richer dynamical behaviors. For this reason, a generalized formulation combining forms (1) and (2) is now introduced as

$$\begin{cases} \dot{X}_i = X_{i+1} \quad \text{for} \quad i = 1 \ldots (n_X - 1) \\ \quad \vdots \\ \dot{W}_i = W_{i+1} \quad \text{for} \quad i = 1 \ldots (n_W - 1) \\ \dot{X}_{n_X} = F_X(X_1, \ldots, X_{n_X}, \ldots W_1, \ldots, W_{n_W}) \\ \quad \vdots \\ \dot{W}_{n_W} = F_W(X_1, \ldots, X_{n_X}, \ldots W_1, \ldots, W_{n_W}), \end{cases} \tag{3}$$

where variables X_1,..., W_1 correspond to the original time series that will be used to build the model; variables X_i,..., W_i $(i \geq 2)$ are their corresponding derivatives; n_X,..., n_W are the maximum derivation numbers used for each variable. The resulting model is of dimension $m = \Sigma n_k$. The univariate form (1) is retrieved by considering one single variable X_1 and its successive derivatives X_i. The simple multivariate model (without derivatives)[15] is retrieved by choosing $n_k = 1, \forall k \in \{X, \ldots, W\}$.

Several important difficulties are met when dealing with the generalized formulation (3). First, contrarily to Eq. (1), the coherence between the whole set of equation is not necessarily guaranteed in itself. Indeed, in Eq. (1), only the last polynomial equation has to be retrieved, whereas the other ones directly result from the data preprocessing of the derivatives. In Eq. (3) (as it was for Eq. (2)), several functions F_k have to be retrieved, and the formulation of the equations must be dynamically coherent to guaranty their numerical integrability. Unfortunately, no definitive algebraic recipe exists to design valid sets of numerically stable equations.

A second difficulty in Eq. (3) arises from the unknown number of derivatives n_X to n_W to be used for each variable. The false nearest neighbors method[49,50] could be used to estimate the dimension of the dynamics, that is, the number of variables necessary to reconstruct the dynamics. This dimension should correspond to m, the sum of the n_k. However, since only low-dimensional approximations can be expected, such an estimate remains of poor use for the present context. Moreover, since no method exists to estimate n_k-values, more empirical approaches will be preferred to fix these parameters. Furthermore, time series are far too short (about fifteen significantly large cycles), noisy and subject to non stationarity to permit such an estimate.

B. Algorithms

A global modeling technique is exclusively based on time series. Therefore, the model dimension m, the numbers of derivatives n_k for each available observable k have to be retrieved on one hand, as well as a proper formulation of the complete ensemble of functions F_k on the other hand. Here, functions F_k are approximated by polynomials. It is thus also necessary to determine their maximum polynomial degree q. Finally, a maximum number n_p^{max} of model parameters is set in order to limit the number of models to explore.

The following algorithm is used to retrieve the model formulation. First, the model dimension m is chosen a priori and all the possible models types are deduced from it, that is, all the structures such as $\Sigma n_k = m$. For example, for a dimension $m = 3$, four possible model general structures have to be explored such as: $(n_X, n_Y) \in \mathcal{E} = \{(0,3), (1,2), (2,1), (3,0)\}$; for a dimension $m = 4$, five possible model general structures such as $(n_X, n_Y) \in \mathcal{E} = \{(0,4), (1,3), (2,2), (3,1), (4,0)\}$, etc. Each of these cases is considered one by one. Each time, n polynomial functions F_k have to be identified, where n is the number of available observables. Since the structures of the polynomials are unknown, they must be retrieved. For a chosen maximum polynomial degree q, the number of possible structures to explore is absolutely tremendous for each function F_k. Therefore, a smaller ensemble of p potential functions must be selected for each function F_k. These functions are chosen by removing the terms of the polynomial structure one by one (a detailed presentation of selection method is given in Ref. 38). For each stage of the structure identification, a Gram-Schmitt procedure is used for precise estimates of the model parameters.[37]

A selection of p potential functions is obtained for each of the n polynomial functions F_k. Therefore, p^n potential models remain to be explored which is still huge. Among these, only the models of size $n_p = \Sigma p_k$ such as $n_p < n_p^{max}$ are kept, where n_p^{max} is the maximum number of parameters allowed. The numerical integrability of this smaller ensemble of models is then systematically tested.

C. Validation

Model validation is a difficult task under chaotic regime since it should be based on quantities independent from the initial conditions. Various properties may be considered to estimate the quality of the model. The comparison between the topological properties of the flow reconstructed from the original data set to the flow of the model obtained by numerical integration can prove that original and modeled dynamics are equivalent. Such validation remains a difficult problem. Indeed, topological characterization is mostly dedicated to three-dimensional dynamical systems.[51,52] Its application to four-dimensional chaotic dynamics remains an emergent task and is considered as a quite difficult problem.[48,51–54] Another difficulty is due to multiplicative noise (or any multiplicative perturbation) that can blur the original flow under real observational conditions, and more especially for environmental observations. Other nonlinear invariants may be chosen. However, the estimation of geometrical and dynamical nonlinear invariants is known to be extremely sensitive to noise and to time series length.[55] Estimates from observational time series could not be sufficiently precise to validate any model in the present epidemiological context.

Other pragmatic approaches will thus be preferred to validate the model. The capacity of the model will be investigated in terms of prediction error, in order to evaluate what level of accuracy can be expected in a forecasting mode. A comparison

Reuse of AIP Publishing content is subject to the terms at: https://publishing.aip.org/authors/rights-and-permissions. Downloaded to IP: 193.51.119.103 On: Thu, 08 Dec 2016 14:23:21

between the variables of the original data and of the model output, and their distributions, will also be performed.

It is important to point out that obtaining a global model producing a flow more developed than the original one is common.[48,56] In fact, this is one of its goal, and this is why global modeling is well adapted for modeling chaos. It is designed—in its principle—to retrieve the equations for the vector field. When the equations are accurately retrieved, they are able to produce the full set of possible solutions and not only the particular solutions from which the global model was obtained.

Nevertheless, altered behaviors may arise due to noisy conditions[36] and to data aggregation[10] which may perturb the selection of the model structure. The lack of observability[57,58] is another important source of difficulty that may blur—or sometimes even hinder—the model identification. Nonetheless, extreme trajectories, although never visited in the original data sets, may be retrieved and can be significant. Theoretically, the global modeling can thus provide useful elements to investigate extreme events without any strong hypotheses about the model dynamics or about the tail of the probability function.

IV. RESULTS AND DISCUSSIONS

A. Phase portraits

The original phase portraits of the dynamics of the West Africa EVD epidemic are presented in Figure 2 (1st and 3rd columns). The negative values observed for X_1^{obs} and Y_1^{obs} correspond to residual inconsistencies that could not be fixed by the data preprocessing (see Section II C for details and discussion). Portrait (a1) shows that the number of new cases of infections per day are overall correlated to the number of deaths, since most of the curve is along the first bisecting line. However, besides this average correlation, important discrepancies are observed between the two variables that reveal, in some cases significant phase shifts (positive shift around day 200, negative one around day 380, see Fig. 1(b)), in other cases a completely different local behavior (around days 340). As a consequence, a complex coevolution may thus be expected between these two variables.

The overall correlation observed between X_1^{obs} and Y_1^{obs} in (a1) leads to similar relations between (X_1^{obs}, Y_2^{obs}) and (Y_1^{obs}, Y_2^{obs}) portraits (Figs. 2(b1) and 2(a3)), characterized

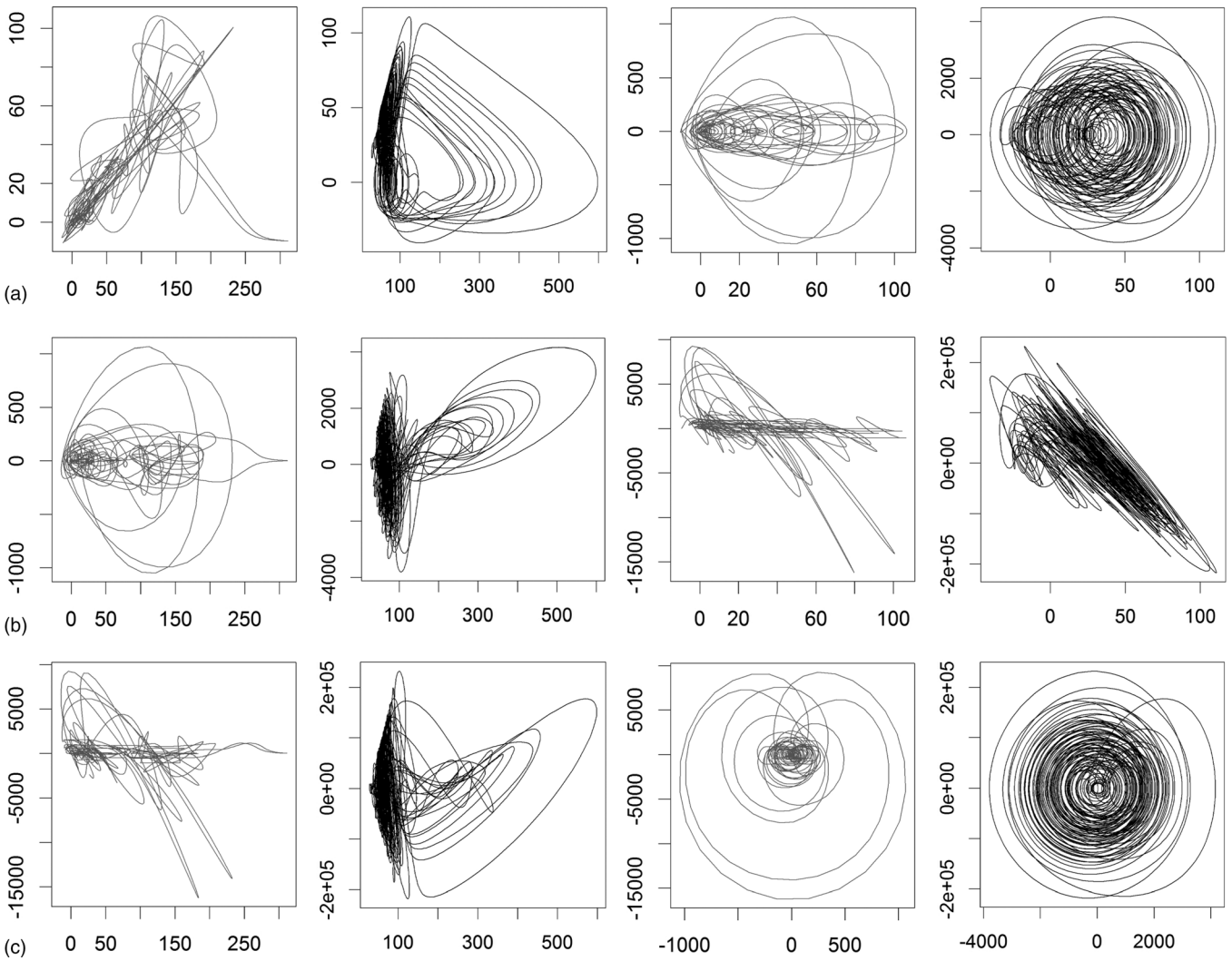

FIG. 2. Projections of the original (columns 1 and 3) and model (columns 2 and 4) phase spaces of the Ebola attractor. Model phase portraits are obtained by numerical integration of the four-dimensional global model (Eq. (4)). Six different projections of the phase space are plotted (a1)–(c4). A blow out of the projection (X_1, Y_1) (3rd column) is also provided (2nd column). (a1) and (a2) correspond to (X1, Y1) portraits, (b1) and (b2) to (X1, Y2), (c1) and (c2) to (X1, Y3), (a3) and (a4) to (Y1, Y2), (b3) and (b4) to (Y1, Y3) and (c3) and c(4) to (Y2, Y3).

Reuse of AIP Publishing content is subject to the terms at: https://publishing.aip.org/authors/rights-and-permissions. Downloaded to IP: 193.51.119.103 On: Thu, 08 Dec 2016 14:23:21

by numerous extended trajectories along the abscissa and a few circular ones. For the same reason, similarities are observed between (X_1^{obs}, Y_3^{obs}) and (Y_1^{obs}, Y_3^{obs}) portraits (Figs. 2(c1) and 2(b3)). For these two projections, most of the trajectories have a long extension along the abscissa whereas a few trajectories exhibit a curved diagonal pattern. Finally, the last portrait (Y_2^{obs}, Y_3^{obs}) in (c3) exhibits cardioid-like structures of irregular amplitudes.

B. A four-dimensional model

The procedure described in Section III B was applied to the window from day 107 to day 411, including the period of rapid progression of the epidemic (see Section II D). Models of dimension $m = 3$ to 5 were investigated for maximum polynomial degrees $q = 2$ to 3 and for maximum size (the parameter maximum number) $n_p^{max} = 20$. The very most of the obtained models were either numerically non integrable, either divergent, or converging to a trivial solution (among these latter, exclusively period-1 cycles were obtained for the present dataset). It may be useful to note that, when unsuccessful, the general formulations revealed quite different levels of inadequacy: most of the formulations among ensembles $\mathcal{E}$ (see Section III B) led to immediate and systematic model rejection (models completely non integrable), whereas few formulations showed to be numerically integrable for long testing periods although finally diverging and thus leading to rejection.

Finally, a single non-trivial integrable model was obtained. This model is a 4-dimensional model (such as $n_X = 1$ and $n_Y = 3$) producing an attractor of complex structure. This model reads

$$\begin{cases} \dot{X}_1 = a_1 Y_1 Y_3 + a_2 Y_1^2 - a_3 X_1 Y_1 \\ \dot{Y}_1 = Y_2 \\ \dot{Y}_2 = Y_3 \\ \dot{Y}_3 = b_1 + \beta b_2 Y_3 + b_3 Y_3^2 - b_4 Y_2 - b_5 Y_2^2 + b_6 Y_1 \\ \qquad -b_7 Y_1 Y_3 + b_8 Y_1 Y_2 - b_9 Y_1^2 - b_{10} X_1 \\ \qquad -b_{11} X_1 Y_3 - b_{12} X_1 Y_2 + b_{13} X_1 Y_1 + b_{14} X_1^2, \end{cases} \tag{4}$$

where parameters a_i and b_i are reported in Table I. The parameter β is a tuning parameter such as $\beta = 1$ by default. This 4D model provides a strong argument for determinism, and, more precisely, for a low-dimensional determinism overriding the dynamics of this epidemic.

The detection of such low-dimensional deterministic model suggests that societal and environmental conditions were quite conducive to the propagation of the epidemic: once the epidemic had broken out, its propagation was largely determined, and probably driven by predominant processes, and possibly few ones.

TABLE I. Parameter values a_i and b_i for the four-dimensional global model (Eq. (4)). By default, β is equal to 1.

a_1	$1.0894896\ 10^{-4}$	b_4	1921.271852	b_{10}	17867.66051
a_2	1.4135051035	b_5	0.1614398401	b_{11}	0.06616088061
a_3	0.9815931187	b_6	34650.56048	b_{12}	24.91575291
b_1	5791.076327	b_7	0.057295177	b_{13}	300.3855818
b_2	3.744720590	b_8	14.52947493	b_{14}	179.1636118
b_3	$2.2511395\ 10^{-5}$	b_9	1056.142579		

The obtained model has four fixed points

$$\begin{matrix} Q_1(\alpha_1, 0, 0, 0), & Q_2(\alpha_2, 0, 0, 0), \\ Q_3(\alpha_3, \alpha_3', 0, 0) & \text{and} \quad Q_4(\alpha_4, \alpha_4', 0, 0), \end{matrix} \tag{5}$$

with $\alpha_1 \approx 99.403$, $\alpha_2 \approx 0.325$, $\alpha_3 \approx -0.240$, $\alpha_3' \approx -0.167$, $\alpha_4 \approx 198.194$ and $\alpha_4' \approx 137.634$. Their classification can be deduced from the eigenvalues Λ_{Q_i} of the Jacobian matrix J linearized at their location Q_i (see supplementary material for details).

For Q_1, two sets of conjugate complex numbers are obtained such as $\Lambda_{Q_1} = (c_1 + d_1 i, c_1 - d_1 i, e_1 + f_1 i, e_1 - f_1 i)$, with real components $c_1 < 0$ and $e_1 > 0$. This point is thus a double-focus point, one focus being stable, the other being unstable.

For Q_2, one set of conjugate complex eigenvalues and two real eigenvalues are obtained such as $\Lambda_{Q_2} = (c_2 + d_2 i, c_2 - d_2 i, e_2, g_2)$, with $c_2 < 0$, $e_2 > 0$ and $g_2 < 0$. This is thus a focus-saddle point.

For Q_3 and Q_4, only real eigenvalues are obtained such as $\Lambda_{Q_3} = (c_3, d_3, e_3, g_3)$ and $\Lambda_{Q_4} = (c_4, d_4, e_4, g_4)$. These points are both saddle points. Only one single direction is stable for Q_3 since only $c_3 < 0$. This point will not have a direct signification since its location corresponds to negative values of X_1 and Y_1. Two directions are stable for Q_4 since both $e_4 < 0$ and $g_4 < 0$.

The attractor obtained from Eq. (4) is shown in Figure 2 (columns 2 and 4) for various projections (transients were removed). The attractor exhibits a quite complex behavior. A region of the phase space of "triangular" shape (left of $X_1 Y_1$-plane projections, Figs. 2(a2)–2(c2)) with a high density of trajectories. Oscillations in this region are relatively moderated in amplitude ($X_1^{max} \lesssim 140$). The observational data mostly belongs to this domain of the phase space (see Fig. 2, 1st column).

The other part of the attractor is associated with larger oscillations of variable X_1 which are quite sparse and are not observed in the original portrait (Fig. 2, 1st column). Quite extreme values of X_1 are obtained in the simulations, up to 600 infections per day. Very punctually these can reach values up to 1200 infections per day with longer simulations. Contrary to this, the largest values reached by Y_1 are almost never beyond 175 deaths per day.

Some patterns can be retrieved in both observed and modeled portraits. In (a2), the linear relation observed in (a1) between X_1^{obs} and Y_1^{obs} in the "triangular" region is retrieved, despite a significantly steeper slope obtained. The rare anti-correlated trajectories observed in the original portrait are likely to correspond to the other type of oscillations which do not belong to the "triangular" region. In the simulations, these can have very large amplitudes along X_1 axis as observed in (a2). In (b2) and (c2), both extended and circular trajectories observed in (b1) and (c1) are more or less retrieved, although strongly altered in shape. In (a4) and (b4), the extended trajectories observed in (a4) and (b3) along Y_1^{obs} axis are difficult to identify, especially in (b4). Contrarily, circular trajectories in (a3), and diagonal ones in (b3) are clearly retrieved in (a4) and (b4). Finally, a good

Reuse of AIP Publishing content is subject to the terms at: https://publishing.aip.org/authors/rights-and-permissions. Downloaded to IP: 193.51.119.103 On: Thu, 08 Dec 2016 14:23:21

coherency is observed between (c3) and (c4), for which cardioid-like patterns can be observed in both portraits.

The spectrum of Lyapunov exponents[59] of the model dynamics was estimated. Their values clearly reveal the high sensitivity of the dynamics to initial conditions ($\lambda_1 \gg 0$): $\lambda_1 = 2.62 \pm 0.03$, $\lambda_2 = 0.02 \pm 0.03$, $\lambda_3 = -1.87 \pm 0.03$, $\lambda_4 = -30.2 \pm 0.06$). The two necessary conditions—determinism, and high sensitivity to initial conditions—are thus retrieved together in a synthetic formulation (Eq. (4)) and provide a strong argument for a low-dimensional chaotic underlying dynamics. As seen in a (X_1, Y_1)-portrait, close trajectories at low values of infection (at the beginning of new flare-up episode) tend to diverge; and tend to converge at the end of each episode. The closeness of the trajectories at the beginning of new flare-ups suggests that actions for slowing down the propagation of the disease (by avoiding or minimizing its transmission at the earliest stages of the infections) can be of high efficacy. This observation is in full agreement with the preventive and control measures put in place by the health community to trace back the cases of infections and deaths to prevent the dissemination of the disease. It also strengthens the importance not to leave any detected case of infection or death under careful observation and control.

The spectrum of Lyapunov exponents can also be used to estimate the fractal dimension of the attractor.[60] This invariant was proven to be well adapted to global modeling.[13] The Kaplan-Yorke dimension is defined as

$$D_{KY} = k + \frac{\sum_{i=1}^{k} \lambda_i}{|\lambda_{k+1}|}, \tag{6}$$

where k is the maximum value such as $\sum_{i=1}^{k} \lambda_i > 0$. In the present case we get $D_{KY} \approx 3.03$. The Ebola attractor is thus clearly four-dimensional but strongly dissipative since D_{KY} is such as $d - 1 < D_{KY} \ll d$, where $d = 4$ is the model dimension. To characterize the structure of the attractor, the Poincaré section

$$P = \{(X_1, Y_1, Y_3) \in \mathcal{A} \subset R^4 / Y_2 = 0, Y_3 < 0\}, \tag{7}$$

was chosen, where $\mathcal{A}$ designates the Ebola attractor. The resulting section is plotted in Figure 3(a). A first return map is usually used to distinguish folding from tearing mechanisms in chaotic attractors.[52,61] To do so, the map is expected to be surjective which is completely impossible for a three-dimensional Poincaré section. To analyze the first return map of the section P plotted in Figure 3(a), an alternate approach based on color tracer is used.[48] To simplify the visualization of the underlying structure, the diffeomorphism

$$\tilde{X}_1 = X_1; \quad \tilde{Y}_1 = Y_2; \quad \tilde{Y}_3 = Y_3 + 2500\, Y_1, \tag{8}$$

is first applied to section P (Eq. (7)), leading to section $\tilde{P}$. To analyze the first return mapping of this section to itself, a color tracer is applied at time t. Its representation $\tilde{P}_t$ is shown in Figure 3(c). Color tracers are then propagated backward into $\tilde{P}_{t-1}$ (Fig. 3(b)) and forward into $\tilde{P}_{t+1}$ and $\tilde{P}_{t+2}$ (Figs. 3(d) and 3(e)). The existence conditions for a suspension states that, for a section in R^m, the suspension should be in R^{m^*} with either $m^* = m + 1$ or $m^* = m + 2$.[48,54] Since m and m^* are known here ($m = 3$ and $m^* = 4$), the model structure should be represented as a branched 3D-manifold embedded in a four-dimensional space. To distinguish it from the so called template (a branched 2D-manifold embedded in a 3D space), this structure will be called a "skeleton".

The visual analysis of the transition from $\tilde{P}_{t-1}$ to $\tilde{P}_t$ provides most of the information about the mapping.[48] First, the continuous limit between the light green (noted A_1) and the light red (noted B) in $\tilde{P}_{t-1}$ becomes discontinuous (A'_1 and B') in $\tilde{P}_t$: it reveals the presence of a tearing mechanism in the attractor. The torn branch (A) becomes the two folded branches (A'_1) and (A'_2). One goes to the upper side of the section, the other one to its lower side. A torsion clearly takes place between A'_1 and A'_2 as indicated by the normal vectors to the two surfaces ($\vec{n}_1$ and $\vec{n}_2$) from the initial section, to the next return ($\vec{n'}_1$ and $\vec{n'}_2$). Second, branch (B) replaces branch (A). The transition from $\tilde{P}_t$ to $\tilde{P}_{t+1}$ mostly shows that branch (A'_1) becomes (A''_1), whereas transition from (B') to (B'') just confirms the behavior revealed by (A). The transition from $\tilde{P}_{t+1}$ to $\tilde{P}_{t+2}$ enables to illustrate the successive accumulation of branches issuing from region A_2 on the top of the structure (C''', A'''_1, B'''_1, etc.).

Based on these observations, a four-branch structure of the Ebola attractor is sketched in Figure 4(a), showing the successive transformations of the section $\tilde{P}$ to come back to itself in a space tangent to the attractor in the phase space. Four branches are necessary to characterize the attractor that

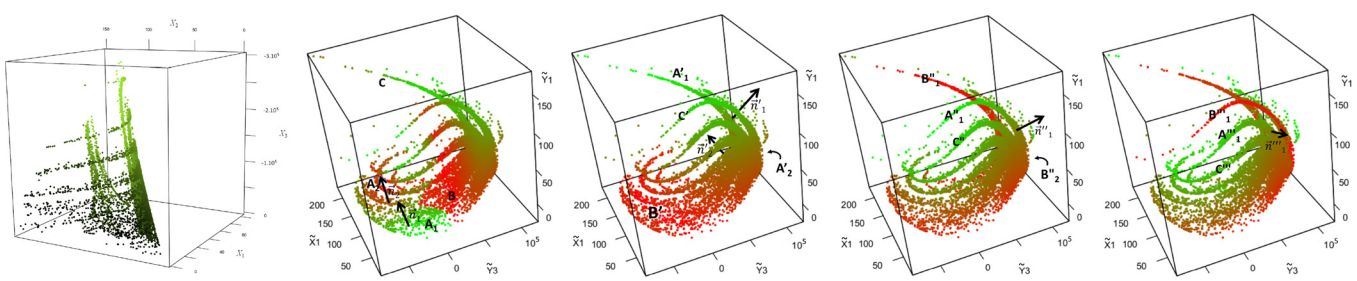

(a) P (b) $\tilde{P}_{t-1}$ (c) $\tilde{P}_t$ (d) $\tilde{P}_{t+1}$ (e) $\tilde{P}_{t+2}$

FIG. 3. (a) Poincaré section P to the Ebola attractor $\mathcal{A}$ (its definition is given in Eq. (7)). Colored values in (a) aim to better distinguish the 3D shape of the section. Section $\tilde{P}$ diffeomorphic to section P based on Eq. (8) is also presented at different times using a color tracer that is propagated from one section to the next return: $\tilde{P}_{t-1}$ in (b), $\tilde{P}_t$ in (c), $\tilde{P}_t$ in (d) and $\tilde{P}_{t+2}$ in (e). To facilitate the analysis, three main regions noted A_1, A_2, and B are selected in $\tilde{P}_{t-1}$. Their propagations are noted with simple and multiple primes in $\tilde{P}_t$ and next $\tilde{P}_{t+1}$ and $\tilde{P}_{t+2}$. Two arrows provide the normal to regions A_1 and A_2 and their propagation in their next return in order to clearly illustrate the foldings, one remaining visible, another one disappearing inside the section.

Reuse of AIP Publishing content is subject to the terms at: https://publishing.aip.org/authors/rights-and-permissions. Downloaded to IP: 193.51.119.103 On: Thu, 08 Dec 2016 14:23:21

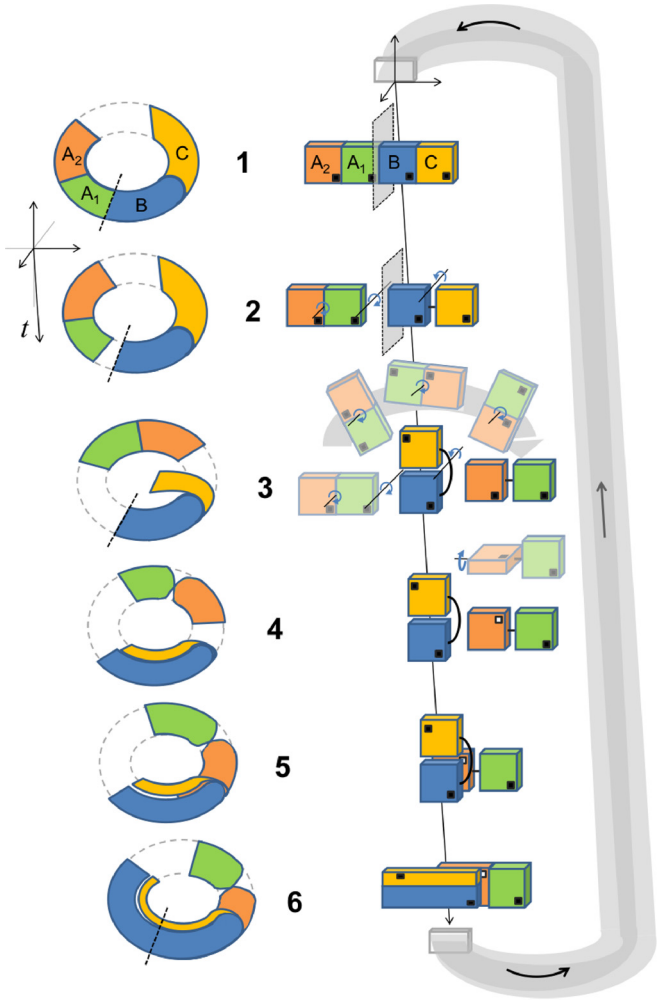

FIG. 4. (a) Structure of the Ebola attractor deduced from the propagation of the color tracer from the Poincaré section to itself. (b) The corresponding skeleton.

implies three boundaries: one corresponds to a tearing (A_1–B), the other two ones to folding A_1–A_2 and B–C. Three hyper-axes of rotation are involved in this evolution, one for each folding and another one between A_{1-2} and B–C. This latter rotation leads to a 4D toroidal structure (partly incomplete). Note that another hyper-axis of rotation is associated with the rotation of the section which maps onto itself.

Extending this toroidal structure along one horizontal axis, a skeleton providing a synthetic characterization of the topological structure of the Ebola attractor is shown in Fig. 4(b).

C. Model validation

The numerical robustness of the model was tested on a long integration run. It was found to be numerically quite stable since integrable on a duration of 250 years, at least, and to be not trivial since it did not converge onto a periodic solution after such a long integration time. It was also observed that the model remains chaotic for a large range of parameter values. This question was investigated by modifying parameter β, that is, on the influence of variable Y_3 which corresponds to the second derivative of Y_1. In mechanics, it may correspond to a force that would control the position Y_1. Since Y_3 is alternately positive and negative, varying parameter β either tends to foster (for $\beta > 1$) or to weaken (for $\beta < 1$) the amplitude of the oscillations. This parameter was varied on the range $\beta \in [0.5; 1.5]$ to compute the bifurcation diagram shown in Figure 5. For $\beta < 0.7$, periodic oscillations of very small amplitude ($X_1 \approx 50$) are obtained, whereas for $\beta > 1.35$ very large ones are obtained ($X_1 > 350$). In between, chaotic behaviors are observed, with sudden transitions (crisis) at both extremities ($\beta = 0.7$ and $\beta = 1.35$).

For most of these chaotic ranges ($\beta \in [0.7, 1.35]$), X_1-values are distributed in the range $[25, 450]$ with a high probability in the range [40, 150]. From a clinical point of view, this means that small parameter changes can only have a limited effect on the dynamical behavior and only a drastic change could affect the propagation of the EVD. Practically, these very large bands of chaotic conditions contribute to explain the difficulty to control and/or to forecast the epidemic. A clear difference of behavior is observed only for two short windows in the bifurcation diagram. One is located at $\beta \approx 1.1$, for which moderate maxima are observed ($X_1 < 150$) but for which minimum values become grater than 60. Another one is located around $\beta \approx 1.22$ for which behavior is also chaotic although trajectories remain concentrated in the neighborhood of a period-4 orbit. These situations are interpreted as a result of a resonance occurring between the main dynamical variables involved. Such almost periodical behavior could probably not be observed under real conditions.

To validate the model, its forecasting ability was tested. To do so, a large set of forecasts was generated starting from successive initial conditions directly taken from the original data set. For each forecast $W(t+\tau)$, where W represents one of the four variables of the system, the error growths $e_W(\tau)$ defined as

$$e_W(t,\tau) = W(t+\tau) - W^{obs}(t+\tau), \tag{9}$$

is estimated, where τ is the prediction horizon. The absolute values $|e_W(\tau)|$ for each of the simulations are plotted (in light gray) in Figure 6. To characterize the error growth statistically, quantiles corresponding to probabilities of 75%, 90%, and 95% are estimated and superimposed over the plots. A

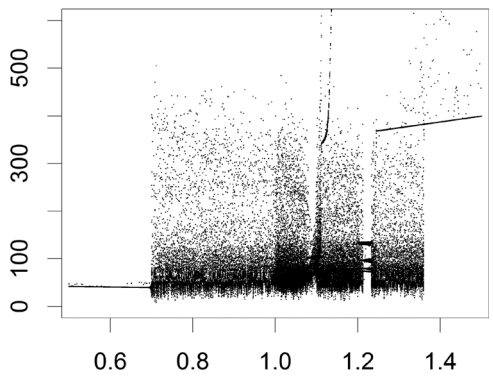

FIG. 5. Bifurcation diagram of X_1 for parameter $\beta \in [0.5; 1.5]$ (see Eq. (4)). The Poincaré section defined in Eq. (7) was used.

Reuse of AIP Publishing content is subject to the terms at: https://publishing.aip.org/authors/rights-and-permissions. Downloaded to IP: 193.51.119.103 On: Thu, 08 Dec 2016 14:23:21

very rapid increase of the error is observed for the earlier (1–2 days) prediction horizon in Figs. 6(a) and 6(d) whereas a slower growth is observed in Fig. 6(b) and to a lesser extent in Fig. 6(c). This behavior directly results from the model formulation that guarantees the initial conditions for the derivatives of Y_1 and Y_2 (2nd and 3rd equations in Eq. (4)), but not for X_1 and Y_3.

In practice, the horizon of predictability will strongly depend on the targeted threshold error and on the accepted level of confidence. For a rather restrictive error threshold, here arbitrarily taken equal to 150 infections per day for X_1 and 50 deaths per day for Y_1, horizons of predictability will be $h_{X_1} = 8$ days and $h_{Y_1} = 4$ days (for a confidence level of 90%).

Prediction error will also vary as a function of time, in particular, from one stage of the epidemic to another. This is clearly illustrated in Fig. 7 where the error $|e_W(t, \tau)|$ is plotted for X_1 and Y_1 as a function of time t in abscissa and of prediction horizon τ in ordinate. Low forecasting errors are systematically observed for short prediction horizons ($\tau \in [5, 10]$ days). Contrary to this, important differences are observed for larger prediction horizons: low levels of error are observed during the earlier period (before day 220) that is during the earlier development of the epidemic while Ebola disease remained located in remote areas. For the second period (days 240 to 350 in particular), while the disease was completely out of control, very heterogeneous patterns of predictability are observed with rapid changes from one day with a very short horizon of predictability to another day with a rather long one. Low levels of error are again

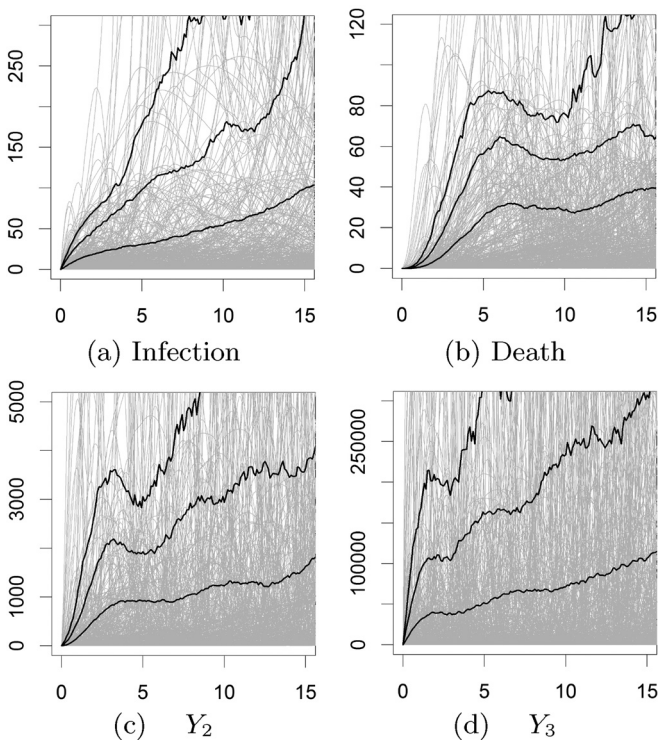

FIG. 6. Absolute error $|e(\tau)|$ of the numbers of infections X_1 (a), deaths Y_1 (b) and of first (c) and second (d) derivatives Y_2 and Y_3 for a large set of initial conditions. Prediction error corresponding to individual trajectories are plotted in light gray. Dark plain lines provide the error level corresponding to a probability of 75% (lower lines), 90% (middle lines), and 95% (upper lines).

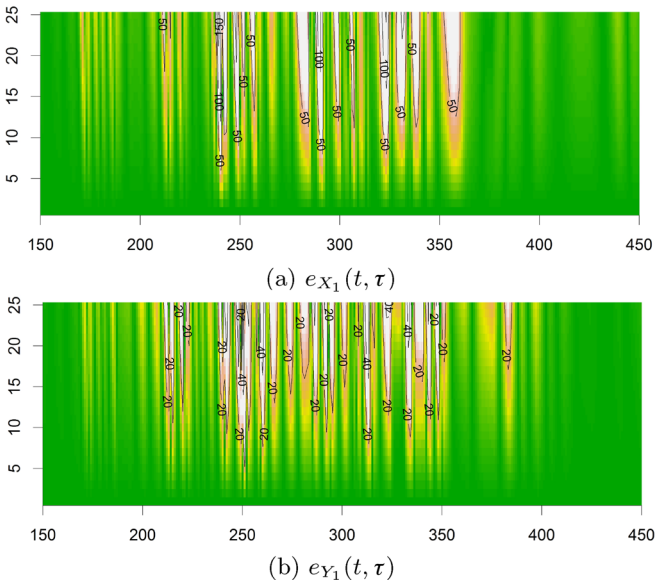

FIG. 7. Prediction error $e(t, \tau)$ for variables X_1 (a) and Y_1 (b); time t is in abscissa, horizon of prediction τ in ordinate, both in day.

observed a few weeks before the decline of the epidemic became detectable (after day 370 for X_1 and after day 390 for Y_1). This shows that the model offers a good level of predictability during the first and third stages of the epidemic (such as $e_{X_1} < 50$ and $e_{Y_1} < 20$), even for long prediction horizons τ. It also suggests that such analysis may help for the early detection of trend changes during an epidemic.

Scatter plots of model predictions versus observations are commonly used to validate models. Because predictions strongly depend on initial conditions as far as chaotic dynamics are concerned, scatter plots are difficult to use for chaotic regimes. Indeed, even if the models were perfect, a lack of precision about the initial conditions would lead to an exponential increase of the error that may completely hinder the utility of a scatter plot for validation. To circumvent this problem, the information about the horizon of prediction should be preserved in the scatter plot. Scatter plots for the four variables are shown in Figure 8 in which colors indicate the prediction time: short horizons of τ are represented in dark grays whereas large ones are in light grays. Ideally, all the dots should be located along the diagonal axis. Due to the sensitivity to initial conditions and to the exponential divergence of the trajectories, the larger the prediction horizon, the more distant from the diagonal lines it may become. For horizons of prediction until 20 days, it is found that rather good levels of prediction can be obtained for the whole range of amplitudes of variables X_1 (Fig. 8(a)) and Y_1 (Fig. 8(b)). Patterns obtained for variables Y_2 and Y_3 are obviously quicker to become noisy (for $\tau \approx$ 5–10 days, typically).

D. Model simulations

The histograms of the four variables of the models at the convergence (thus corresponding to the chaotic attractor presented in Fig. 2) were also compared to the histograms of the original dataset (Fig. 9). Negative values result from residual

Reuse of AIP Publishing content is subject to the terms at: https://publishing.aip.org/authors/rights-and-permissions. Downloaded to IP: 193.51.119.103 On: Thu, 08 Dec 2016 14:23:21

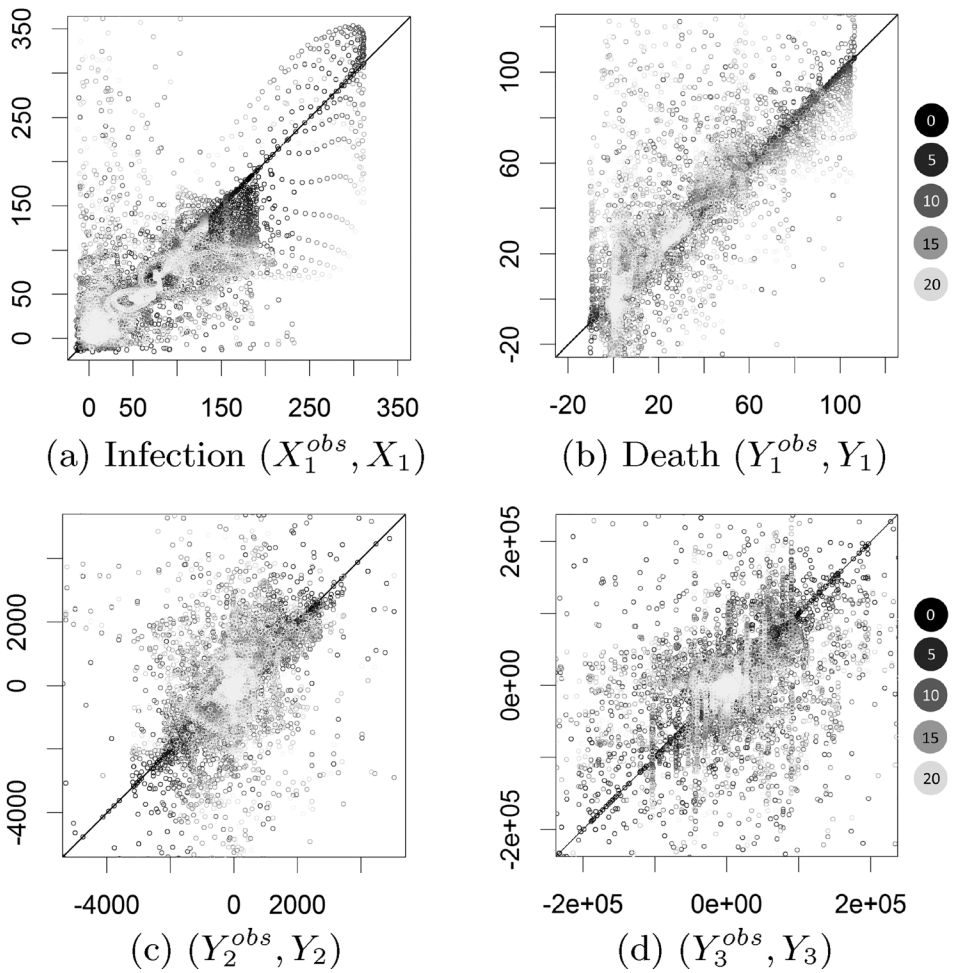

FIG. 8. Scatter plots of the predictions X_1, Y_1, Y_2, and Y_3 as a function of the corresponding observations. Colored values denote the prediction horizon τ (in day).

inconsistencies that could not be fixed by the data preprocessing (see Section II C for details and discussion). It is observed that for both variables X_1^{obs} and Y_1^{obs}, most of the signal is concentrated in the very first part of the distribution: maximum frequency in [0; 25] for X_1^{obs} and [0; 20] for Y_1^{obs}. This huge probability for the lower values directly results from the earlier stage of the epidemic—before the multiplication of new foci outbreak (days 100 to 200)—and from the long breakdown to the end of the epidemic (days 550 to 765), during which daily infection and death rates were slowly vanishing. It is not the case for the attractor for which peaks correspond to significantly positive values (in the range [25; 50] for X_1, and [20–40] for Y_1, Figs. 9(c) and 9(d), dashed line). Since variable X_1 always remains positive, the dynamics on the attractor can obviously correspond neither to the earlier development of the disease, nor to the end of the epidemic. Its behavior corresponds to the 2nd stage of the epidemic, that is before human action became sufficient for slowing down the propagation of the disease. To compare this dynamics to the observations in a proper fashion, observational distributions were thus reevaluated for the period spanning from day 230 to day 560 excluding the earlier and the later evolution of the epidemic. A good agreement between the data and attractor distributions is found for this period that provides a statistical element of validation of the model and shows that the behavior on the attractor belongs to the second stage of the epidemic.

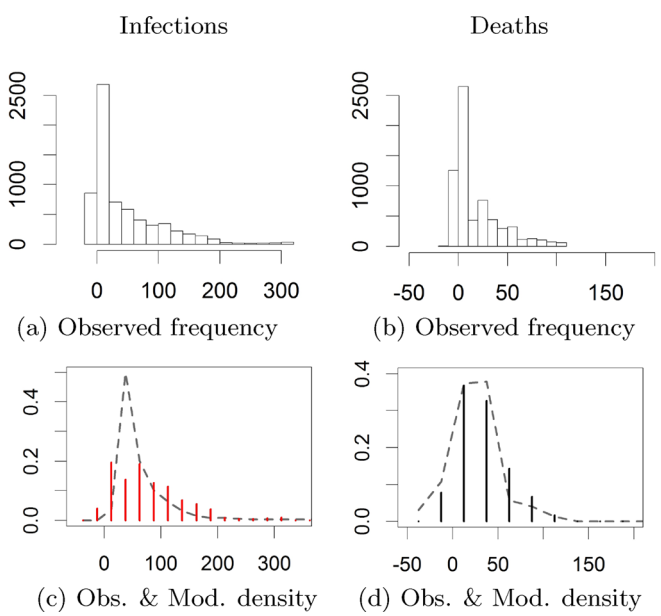

FIG. 9. Statistical distributions of the daily numbers of infections and deaths. Histograms obtained for the original variables X_1^{obs} and Y_1^{obs} are shown, respectively, in (a) and (b), for the complete data period available (days 111 to 775). Densities obtained for the simulations of X_1 and Y_1 are plotted in (c) and (d) (dashed lines). Observed data densities are also reported as bars. A selective period (days 230 to 560) is used for the observed data.

Reuse of AIP Publishing content is subject to the terms at: https://publishing.aip.org/authors/rights-and-permissions. Downloaded to IP: 193.51.119.103 On: Thu, 08 Dec 2016 14:23:21

The obtained model being autonomous in its formulation, a simulation initiated with very low numbers of infections and deaths could be performed. Since the earlier developments of this epidemic was not recorded, the model cannot be initiated using real initial conditions. In practice, the following sets of initial conditions $W_0 = (X_1, Y_1, Y_2, Y_3)$ were used to generate two simulations of the earlier development of the epidemic: $W_0' = (1, 1, 100, 5000)$ and $W_0'' = (1, 1, 100, 4000)$. These simulations are presented as light lines in Figure 10. The quick divergence observed between the trajectories issued from W_0' and W_0'' also provides a direct illustration of the high sensitivity to initial conditions. Obviously, these initial conditions do not belong to the chaotic attractor since the trajectory will never come back to its close vicinity (the smallest values reached during the 250 year long simulation were always such as $X_1 \geq 13$). This is another confirmation that the attractor is more characteristic of the period of plain progression of the epidemic.

The two-year long simulation of variable X_1 shown in Figure 10(a) is very complex. It includes punctual flare-ups of quite high magnitudes characterized by numbers of daily cases that commonly reach 200 to 700 infections per day. Such flare-ups are generally followed by periods characterized by quite irregular variations around relatively high averaged levels ($X_1 > 100$ cases per day) and from which strong flare-ups may re-emerge. Situations of lower levels of epidemic ($X_1 < 100$ cases per day) can also be observed, possibly over a long period during which epidemic remains active. Such behavior appears coherent with the behavior observed at the end of the epidemic, while health services were struggling to halt the epidemic but during which punctual cases of infections could always re-appear. However, the averaged level of infection per day is clearly overestimated by the model.

The behavior of variable Y_1 appears less realistic in amplitudes since negative values are commonly reached (Fig. 10(b)). Negative values probably result from a too coarse algebraic formulation of the dynamical equations. However, this approximation may not necessarily alter the topology of the dynamics. Indeed, a similar situation was noted when modeling the epidemic of plague in Bombay.[15] Several models were obtained, the simplest one was a 10-term model for which an interpretation was proposed for each algebraic term. It was found that the drawbacks of the simplest 10-term model were mostly corrected by adding appropriate algebraic terms that did not alter the topology of the attractor, but mainly improved the magnitudes of the variables and avoided negative values.

From a dynamical point of view, it is also observed that during the outbreak, flare-ups can act as shocks that will generate oscillations in the number of deaths in response to strong perturbations. This behavior can be interpreted as a resonance effect. Such behavior was previously observed in a theoretical case in response to massive vaccination playing as shocks.[62]

The comparison between the observed and simulated time series also shows a relatively good agreement. Of course, the correspondence in time is somehow fortuitous. Indeed, the dynamics being chaotic, the high sensitivity to initial conditions cannot guarantee any synchronicity. Nonetheless, this superposition shows that short time scale oscillations (7–13 days) observed in both variables (plain lines) are partly retrieved in the simulations (light lines). Note that the long oscillation cycle observed in the data (from days 200 to 500) is also roughly reproduced by the simulations. It also reveals that the first flare-ups of very high strength can typically be expected 150–250 days after the first case: this is in agreement with the observations. Note also that the characteristic time between groups of flare-ups (e.g., between day 320 and day 580 in Fig. 10(a)) is of similar length.

The cumulative counts of infections and deaths presented in Figure 11 were deduced from the run generated from initial condition W_0'. During the earlier period (days 110–300), estimates of cumulative counts are slightly too low for X_0 and clearly underestimated for Y_0. The quicker start that was observed in Figure 10 is thus retrieved here. Obviously, the

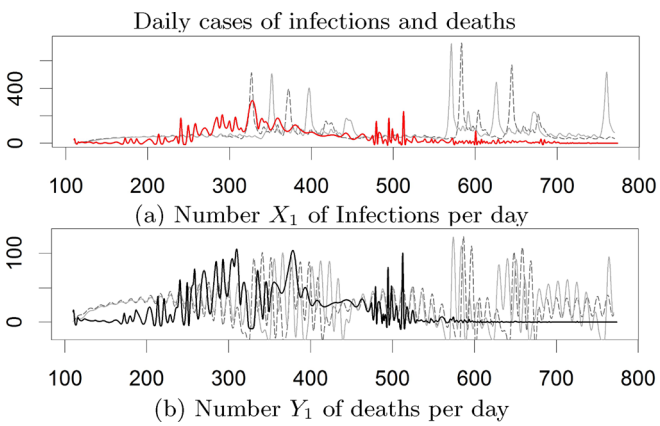

FIG. 10. Comparison between modeled and observed daily cases of infections and deaths, per day: Numbers of infections (a) and deaths (b) per day estimated by the model from two initiations conditions W_0' and W_0' (dashed and plain gray lines) and observed (bold lines).

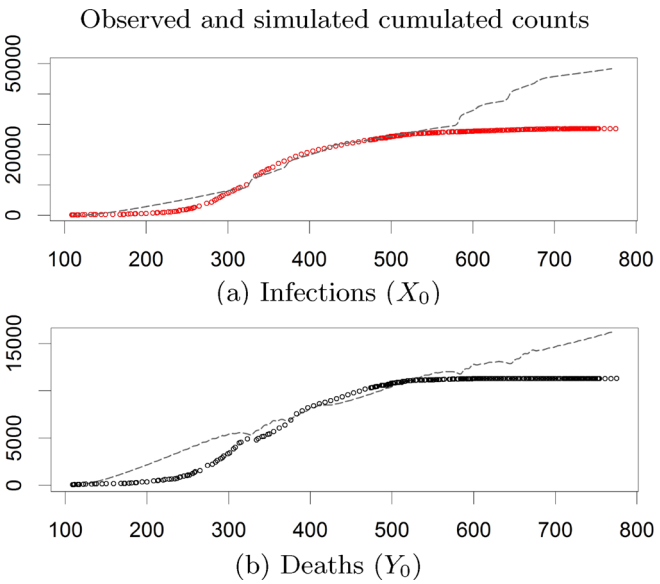

FIG. 11. Comparison between the modeled and observed cumulative cases of EVD infections and deaths: Cumulative numbers of Infections (a) and of deaths (b) estimated by the model (dashed gray lines) and observed (plain lines).

Reuse of AIP Publishing content is subject to the terms at: https://publishing.aip.org/authors/rights-and-permissions. Downloaded to IP: 193.51.119.103 On: Thu, 08 Dec 2016 14:23:21

model appears more adapted to simulate the trend of the propagation of the disease during the second stage of the epidemic (days 300 to 500), while EVD was propagating in areas denser in population. During the last stage, the epidemic is progressively slowed down, thanks to the response by the health services until its end whereas the model keeps the same trend corresponding to a stationary regime.

It is observed that, depending on the type of analysis, the model is able to well reproduce the general trend particularly during the second stage of the disease (Fig. 11). During the third stage, the propagation returns back under control. For this reason, events of low predictability become rarer and the behavior easier to forecast again.

These three stages can thus be explained by a succession of temporarily stationary stages, similar to what was observed when modeling the dynamical behavior of plague epidemic in Bombay.[15] The model obtained here for the epidemic of EVD most likely corresponds to the second period, while actions to stop the disease remained insufficient to halt its propagation.

Being stationary in its formulation, a chaotic attractor can bring useful information about how the propagation of the disease would evolve without stronger human action to stop the disease. Based on this simulation (Fig. 11), it can be estimated that, without the measures taken to stop the epidemic, it could have continued its quick propagation at an average speed of $\approx$26 800 infections per year and $\approx$9300 deaths per year. These magnitudes are in coherence with previous estimates.[63,64]

V. DISCUSSION AND CONCLUSION

A generalized version of the global modeling technique was developed and applied to the epidemic of EVD that occurred in West Africa from 2013 to 2016. Only two time series were used in the present analysis: the counts of confirmed infections and deaths. The model equations were obtained from observational time series, without any a priori information about the equation forms and parameterization.

The ability of the model to simulate the dynamics was evaluated by comparing the model simulations to the observations based on various representations (phase portraits, error growth, scatter plots, statistic distributions, etc.) providing a complete illustration of the model skills and drawbacks.

The generalized global modeling approach permitted to obtain a model able to produce very long simulations proving that the model is numerically robust. Obtaining a set of equations numerically integrable for a long duration, and for a behavior corresponding to an extremely intense stage of the epidemic, suggests that, for the considered stage, human action to stop the propagation of the disease remained unadapted or, more likely, insufficient in its strength or in its organization. This situation is the result of numerous reasons that were already evoked: strongly predisposed context in which Ebola virus could easily propagate, poorly known mode of contamination, unprecedented and thus fully unprepared health services and populations, etc. Such simulations may probably be not realistic on very long time scales since, being stationary, the present model cannot take into account long term effects of immunization and selection that would let evolve the behavior. The model can however provide insights about the immediate evolution of the epidemic (at a short time scale of 0–10 days) and about its general trend (considering cumulative counts). It can also be used to distinguish the different stages of the epidemic.

When considering the sigmoidal shape of the cumulative counts of infections and deaths (Fig. 1(a)), the time evolution of the epidemic appears quite simple. On the contrary, the chaotic model here obtained gives a strong argument for a quite complex dynamical behavior, in particular, during the second stage of uncontrolled behavior. The model illustrates the possibility for such a complex dynamics to take place in real epidemiological conditions.

To obtain a chaotic model for the EVD directly from observational data brings a strong and direct argument for chaos and suggests that the propagation of the disease is firstly due to low-dimensional deterministic processes, although stochastic-like contributions may also play a role of second order in the propagation of the disease. Several processes at work in the propagation of the disease were clearly identified.[65] Among these, the contact with the dead bodies during traditional burials have been proven to have a direct role in the propagation of EVD[5,22] that can contribute to explain such low-dimensional behavior.

For some diseases, the key actors of the epidemic can be identified beforehand. In such cases, the development of a survey can be facilitated if the actors can accept the surveillance system.[66,67] In the case of EVD epidemics, the key actors are numerous and very diversified,[5,21,65] and thus difficult to prepare beforehand. Moreover, the acceptance by the population of clinical and epidemiological measures may be both challenging and uncertain.[6,11,22] The development of an early alert system under such conditions appears really challenging.

Obtaining a chaotic model underlines the high sensitivity to initial conditions. From a dynamical point of view, this result is important since it proves that, without control, any undetected case may lead to an exponential increase of the number of infections. The development of an early alert system should take this property into account as a problem of first importance. In the case of a chaotic behavior, and more especially for a lethal disease such as EVD for which no prophylactic and therapeutic strategies are available, an alert system based on a tracing back is very likely the only way to stop an epidemic.

From a dynamical system point of view, obtaining four-dimensional chaotic models directly from observational data is rare. It should be emphasized that, to be considered as valid, a chaotic model has to be numerically integrable for a long time and should not converge onto a trivial solution. To the best of our knowledge, only two cases of four-dimensional chaotic models obtained from observed data were reported: one for a mixing reactor where the data were obtained from a controlled experiment in laboratory;[44] and another one for the cycles of Lynx in Canada,[12] although this latter model could unfortunately not be integrated during an extensively long duration. In this sense, the present Ebola

Reuse of AIP Publishing content is subject to the terms at: https://publishing.aip.org/authors/rights-and-permissions. Downloaded to IP: 193.51.119.103 On: Thu, 08 Dec 2016 14:23:21

attractor is probably the first four-dimensional attractor directly obtained from the real environmental world.

Topology of chaos has proven to be a powerful way to characterize dynamical systems.[51] However, the topological analysis of four-dimensional chaos remains a quite difficult problem today.[52] A topological characterization of a four-dimensional chaos is provided here. It is shown that the structure of the Ebola attractor reduces to four branches only, corresponding to specific situations during the propagation of the epidemic. Its four-dimensional structure involves folding mechanisms that cannot take place in a three-dimensional space (such as double rotations) and that cannot be sketched by a traditional template.

SUPPLEMENTARY MATERIAL

See supplementary material for details concerning the fixed points of the Ebola model (Eq. (4)).

ACKNOWLEDGMENTS

This work was supported by the French National Programs LEFE/INSU and InPhyNiTi/CNRS. The authors would like to thank the two anonymous reviewers for their constructive suggestions. S. Mangiarotti wishes to thank Christophe Letellier for stimulating discussions.

[1]W. O. Kermack and A. G. McKendrick, "A contribution to the mathematical theory of epidemics," Proc. R. Soc. London A **115**, 700–721 (1927).
[2]J. Shaman, W. Yang, and S. Kandula, "Inference and forecast of the current West African Ebola tweet outbreak in Guinea, Sierra Leone and Liberia," PLOS Curr. Outbreaks **6**, Oct. 31 (2014).
[3]C. M. Rivers, E. T. Lofgren, M. Marathe, S. Eubank, and B. L. Lewis, "Modeling the impact of interventions on an Epidemic of Ebola in Sierra Leone and Liberia," PLOS Curr. Outbreaks **6**, Nov. 6 (2014).
[4]A. Camacho, A. J. Kucharski, S. Funk, J. Breman, P. Piot, and W. J. Edmunds, "Potential for large outbreaks of Ebola virus disease," Epidemics **9**, 70–78 (2014).
[5]J. Legrand, R. F. Grais, P. Y. Boelle, A. J. Valleron, and A. Flahault, "Understanding the dynamics of Ebola epidemics," Epidemiol. Infect. **135**(4), 610–621 (2007).
[6]K. A. Alexander, C. E. Sanderson, M. Marathe, B. L. Lewis, C. M. Rivers *et al.*, "What factors might have led to the emergence of Ebola in West Africa?," PLoS Neglected Trop. Dis. **9**(6), e0003652 (2015).
[7]Centers for Disease Control and Prevention, see http://www.cdc.gov/vhf/ebola/outbreaks/history/ distribution-map.html for Cases of Ebola Virus Disease in Africa, 1976–2015 (last accessed 15 June 2016).
[8]H. Feldmann and T. W. Geisbert, "Ebola haemorrhagic fever," NIH-PA **377**(9768), 849–862 (2011).
[9]M. D. Van Kerkhove, A. I. Bento, H. L. Mills, N. M. Ferguson, and C. A. Donnelly, "A review of epidemiological parameters from Ebola outbreaks to inform early public health decision-making," Sci. Data **2**, 150019 (2015).
[10]S. Mangiarotti, F. Le Jean, M. Huc, and C. Letellier, "Global modeling of aggregated and associated chaotic dynamics," Chaos, Solitons, Fractals **83**, 82–96 (2016).
[11]O. Cenciarelli, S. Pietropaoli, A. Malizia, M. Carestia, F. D'Amico, A. Sassolini *et al.*, "Ebola virus disease 2013–2014 outbreak in West Africa: An analysis of the epidemic spread and response," Int. J. Microbiol. **2015**, 769121.
[12]J. Maquet, C. Letellier, and L. A. Aguirre, "Global models from the Canadian lynx cycles as a direct evidence for chaos in real ecosystems," J. Math. Biol. **55**(1), 21–39 (2007).
[13]S. Mangiarotti, L. Drapeau, and C. Letellier, "Two chaotic global models for cereal crops cycles observed from satellite in Northern Morocco," Chaos **24**, 023130 (2014).
[14]G. Boudjema and B. Cazelles, "Constructing homoclinic orbits and chaotic attractors," Chaos, Solitons, Fractals **12**, 2051–2069 (2001).
[15]S. Mangiarotti, "Low dimensional chaotic models for the plague epidemic in Bombay (1896–1911)," Chaos, Solitons, Fractals **81**(A), 184–196 (2015).
[16]E. M. Leroy, B. Kumulungui, X. Pourrut, P. Rouquet, A. Hassanin, P. Yaba *et al.*, "Fruit batsas reservoirs of Ebola virus," Nature **438**, 575–576 (2005).
[17]A. T. Peterson, J. T. Bauer, and J. N. Mills, "Ecologic and geographic distribution of filovirus disease," Emerging Infect. Dis. **10**(1), 40–47 (2004).
[18]D. M. Pigott, N. Golding, A. Mylne, Z. Huang, A. J. Henry *et al.*, "Mapping the zoonotic niche of Ebola virus disease in Africa," eLife **3**, e04395 (2014).
[19]K. Norris, A. Asase, B. Collen, J. Gockowksi, J. Mason, B. Phalan, and A. Wadea, "Biodiversity in a forest-agriculture mosaic—The changing face of West African rainforests," Biol. Conserv. **143**, 2341–2350 (2010).
[20]E. M. Leroy, A. Epelboin, V. Mondonge, X. Pourrut, J.-P. Gonzalez, J.-J. Muyembe-Tamfum, and P. Formenty, "Human Ebola outbreak resulting from direct exposure to fruit bats in Luebo, Democratic Republic of Congo," Vector-Borne Zoonotic Dis. **9**, 723–728 (2009).
[21]G. Chowell and H. Nishiura, "Transmission dynamics and control of Ebola virus disease (EVD): A review," BMC Med. **12**, 196 (2014).
[22]Y. Guimard, M. A. Bwaka, R. Colebunders, P. Calain, M. Massamba *et al.* "Organization of patient care during the Ebola hemorrhagic fever epidemic in Kikwit, Democratic Republic of the Congo, 1995," J. Infect. Dis. **179**, S268–S273 (1999).
[23]G. D. Maganga, J. Kapetshi, N. Berthet, B. Kebela Ilunga *et al.*, "Ebola virus disease in the Democratic Republic of Congo," N. Engl. J. Med. **371**, 2083–2091 (2014).
[24]D. G. Bausch and L. Schwarz, "Outbreak of Ebola virus disease in Guinea: Where ecology meets economy," PLoS Neglected Trop. Dis. **8**(7), e3056 (2014).
[25]Centers for Disease Control and Prevention (2014), see http://www.cdc.gov/vhf/ebola/outbreaks/2014-west-africa/previous-case-counts.html for Ebola (Ebola Virus Disease).
[26]S. Baize, D. Pannetier, L. Oestereich, T. Rieger, L. Koivogui *et al.*, "Emergence of Zaire Ebola virus disease in Guinea—Preliminary report," N. Engl. J. Med. **371**, 1418–1425 (2014).
[27]World Health Organization see http://apps.who.int/iris/bitstream/10665/131596/1/EbolaResponseRoadmap.pdf for Ebola Response Roadmap (2014).
[28]A. Savitzky and M. J. Golay, "Smoothing and differentiation of data by simplified least squares procedures," Anal. Chem. **36**(8), 1627–1639 (1964).
[29]World Health Organization (WHO), see http://www.who.int/csr/don/20140808ebola/en/ for Global Alert and Response. Disease Outbreak News. Ebola Virus Disease, West Africa-Update, 2014.
[30]World Health Organization (WHO), see https://storify.com/WHO/who-ebola-situation-report-29-august-2014 for WHO: Ebola Response Roadmap Situation Report 1, 2014.
[31]World Health Organization (WHO), see http://www.who.int/csr/disease/ebola/situation-reports/archive/en/ for Ebola Situation Reports: Archive (last accessed 3 December 2014).
[32]World Health Organization (WHO), see http://www.who.int/csr/disease/ebola/situation-reports/archive/en/ for Ebola Situation Reports: Archive (last accessed 7 January 2015).
[33]World Health Organization (WHO), see http://www.who.int/csr/disease/ebola/situation-reports/archive/en/ for Ebola Situation Reports: Archive (last accessed 14 January 2015).
[34]World Health Organization (WHO), see http://www.who.int/csr/disease/ebola/situation-reports/archive/en/ for Ebola Situation Reports: Archive (last accessed 28 January 2015).
[35]J. P. Crutchfield and B. S. McNamara, "Equations of motion from a data series," Complex Syst. **1**, 417–452 (1987).
[36]C. Letellier, L. A. Aguirre, and U. S. Freitas, "Frequently asked questions about global modeling," Chaos **19**, 023103 (2009).
[37]G. Gouesbet and C. Letellier, "Global vector field reconstruction by using a multivariate polynomial L_2-approximation on nets," Phys. Rev. E **49**(6), 4955–4972 (1994).
[38]S. Mangiarotti, R. Coudret, L. Drapeau, and L. Jarlan, "Polynomial search and global modeling: Two algorithms for modeling chaos," Phys. Rev. E **86**(4), 046205 (2012).
[39]J. D. Farmer and J. J. Sidorowich, "Predicting chaotic time series," Phys. Rev. Lett. **59**(8), 845–848 (1987).
[40]M. Giona, F. Lentini, and V. Cimagalli, "Functional reconstruction and local prediction of chaotic time series," Phys. Rev. A **44**(6), 3496–3502 (1991).

Reuse of AIP Publishing content is subject to the terms at: https://publishing.aip.org/authors/rights-and-permissions. Downloaded to IP: 193.51.119.103 On: Thu, 08 Dec 2016 14:23:21

[41]L. A. Aguirre and S. A. Billings, "Dynamical effects of overparametrization in nonlinear models," Physica D **80**, 26–40 (1995).
[42]G. Gouesbet and J. Maquet, "Construction of phenomenological models from numerical scalar time series," Physica D **58**, 202–215 (1992).
[43]C. Letellier, L. Le Sceller, P. Dutertre, G. Gouesbet, Z. Fei, and J. Hudson, "Topological characterization and global vector field reconstruction of an experimental electrochemical system," J. Phys. Chem. **99**(18), 7016–7027 (1995).
[44]C. Letellier, L. Le Sceller, G. Gouesbet, F. Lusseyran, A. Kemoun, and B. Izrar, "Recovering deterministic behavior from experimental time series in mixing reactor," AIChE J. **43**(9), 2194–2202 (1997).
[45]E. N. Lorenz, "Irregularity: A fundamental property of the atmosphere," Tellus **36A**, 98–110 (1984).
[46]S. Wieczorek, B. Krauskopf, and D. Lenstra, "A unifying view of bifurcations in a semiconductor laser subject to optical injection," Opt. Commun. **172**, 279–295 (1999).
[47]K. E. Chlouverakis and J. C. Sprott, "A comparison of correlation and Lyapunov dimensions," Physica D **200**, 156–164 (2005).
[48]S. Mangiarotti, "Modélisation globale et caractérisation topologique de dynamiques environnementales: de l'analyse des enveloppes fluides et du couvert de surface de la Terre à la caractérisation topolodynamique du chaos," dissertation (Habilitation to Direct Researches, Université de Toulouse, 2014).
[49]M. B. Kennel, R. Brown, and H. D. I. Abarbanel, "Determining embedding dimension for phase-space reconstruction using a geometrical construction," Phys. Rev. A **45**, 3403–3411 (1992).
[50]L. Cao, "Practical method for determining the minimum embedding dimension of a scalar time series," Physica D **110**, 43–50 (1997).
[51]R. Gilmore and M. Lefranc, *The Topology of Chaos* (Wiley, New York) (2002).
[52]C. Letellier and R. Gilmore, "Introduction to topological analysis," in *Topology and Dynamics of Chaos: In Celebration of Robert Gilmore's 70th Birthday*, edited by C. Letellier (World Scientific Publishing Co. Pvt. Ltd., 2013), pp. 1–19.
[53]M. Lefranc, "Alternative determinism principle for topological analysis of chaos," Phys. Rev. E **74**, 035202 (2006).
[54]S. Mangiarotti and C. Letellier, "Topological analysis for designing a suspension of the Hénon map," Phys. Lett. A **379**, 3069–3074 (2015).
[55]M. Ding, C. Grebogi, E. Ott, T. Sauer, and J. A. Yorke, "Estimating correlation dimension from a chaotic time series: When does plateau onset occur?," Physica D **69**, 404–424 (1993).
[56]C. Letellier, E. Ringuet, B. Maheu, J. Maquet, and G. Gouesbet, "Global vector field reconstruction of chaotic attractors from one unstable periodic orbit," Entropie **202/203**, 147–153 (1997).
[57]C. Letellier, L. A. Aguirre, and J. Maquet, "Relation between observability and differential embeddings for nonlinear dynamics," Phys. Rev. E **71**(6), 066213 (2005).
[58]E. Bianco-Martinez, M. S. Baptista, and C. Letellier, "Symbolic computations of nonlinear observability," Phys. Rev. E **91**, 062912 (2015).
[59]A. Wolf, J. B. Swift, H. L. Swinney, and J. A. Vastano, "Determining Lyapunov exponents from a time series," Physica D **16**, 285–317 (1985).
[60]J. L. Kaplan and J. A. Yorke, "Chaotic Behavior of Multidimensional Difference Equations," in *Functional Differential Equations and Approximations of Fixed Points*, Lecture Notes in Mathematics Vol. 730, edited by H.-O. Peitgen and H.-O. Walter (Springer, Berlin, 1979).
[61]C. Letellier, E. Roulin, and O. Rössler, "Inequivalent topologies of chaos in simple equations," Chaos, Solitons, Fractals **28**, 337–360 (2006).
[62]M. Choisy, J.-F. Guégan, and P. Rohani, "Dynamics of infectious diseases and pulse vaccination: Teasing apart the embedded resonances effects," Physica D **223**(1), 26–35 (2006).
[63]D. Fisman, E. Khoo, and A. Tuite, "Early epidemic dynamics of the West African 2014 Ebola Outbreak: Estimates derived with a simple two-parameter model," PLoS Curr. Outbreaks **6**, Sep. 8 (2014).
[64]B. Ivorra, D. Ngom, and Á. M. Ramos, "Be-CoDiS: A mathematical model to predict the risk of human diseases spread between countries. Validation and application to the 2014 Ebola Virus Disease epidemic," Bull. Math. Biol. **77**(9), 1668–1704 (2015).
[65]A. Du Toit, "Ebola virus in West Africa," Nat. Rev. Microbiol. **12**(5), 312 (2014).
[66]K. Schulz, C. Calba, M. Peyre, C. Staubach, and F. J. Conraths, "Hunters acceptability of the surveillance system and alternative surveillance strategies for classical swine fever in wild boar—A participatory approach," BMC Veterinary Research **12**, 187 (2016).
[67]C. Calba, F. L. Goutard, L. Hoinville, P. Hendrikx, A. Lindberg, C. Saegerman, and M. Peyre, "Surveillance systems evaluation: A systematic review of the existing approaches," BMC Public Health **15**, 448 (2015).

Reuse of AIP Publishing content is subject to the terms at: https://publishing.aip.org/authors/rights-and-permissions. Downloaded to IP: 193.51.119.103 On: Thu, 08 Dec 2016 14:23:21